Robustness and Optimality of Light Harvesting in Cyanobacterial Photosystem I

Melih K. Sener,[†] Deyu Lu,[†,‡] Thorsten Ritz,[§] Sanghyun Park,[†,‡] Petra Fromme,[#,⊥] and Klaus Schulten*[,†,‡]

Beckman Institute, University of Illinois at Urbana-Champaign, Urbana, Illinois 61801, Department of Physics, University of Illinois at Urbana-Champaign, Urbana, Illinois 61801, Department of Biology, Virginia Polytechnic Institute and State University, Blacksburg, Virginia 24061, Max-Volmer Laboratorium für Biophysikalische Chemie, Institut für Chemie, Fakultät 2, Technische Universität Berlin, D-10623 Berlin, Germany, Department of Chemistry and Biochemistry, Arizona State University, Tempe, Arizona 85287-1604

Received: March 14, 2002; In Final Form: May 23, 2002

As most biological species, photosynthetic lifeforms have evolved to function optimally, despite thermal disorder and with fault tolerance. It remains a challenge to understand how this is achieved. To address this challenge, the function of the protein−pigment complex photosystem I (PSI) of the cyanobacterium *Synechococcus elongatus* is investigated theoretically. The recently obtained high-resolution structure of this complex exhibits an aggregate of 96 chlorophylls that are electronically coupled to function as a light-harvesting antenna complex. This paper constructs an effective Hamiltonian for the chlorophyll aggregate to describe excitation transfer dynamics and spectral properties of PSI. For this purpose, a new kinetic expansion method, the sojourn expansion, is introduced. Our study shows that at room temperature fluctuations of site energies have little effect on the calculated excitation lifetime and quantum yield, which compare favorably with experimental results. The efficiency of the system is found to be robust against "pruning" of individual chlorophylls. An optimality of the arrangement of chlorophylls is identified through the quantum yield in comparison with an ensemble of randomly oriented chlorophylls, though the quantum yield is seen to change only within a narrow interval in such an ensemble.

1. Introduction

Photosynthesis is the main source of energy in our biosphere. Although light-harvesting systems show a great variety in their design and function, most of them are membrane proteins comprised of a network of pigment antennae surrounding a reaction center.[1] The antenna complex is responsible for the absorption of light and the transfer of the resulting electronic excitation to a so-called special pair of chlorophylls in the reaction center, where a charge separation across the cell membrane is initiated. This charge separation is later utilized by the cell to store energy through synthesis of ATP in a more stable form.

Oxygenic photosynthetic species employ two transmembrane protein−pigment complexes for light-harvesting, named photosystems I and II. Photosystem I (PSI) is a ubiquitous protein−pigment complex found in green plants, algae, and cyanobacteria. Located in the bacterial membrane, it absorbs sun light and uses its energy to transfer electrons across the cell membrane. PSI is remarkable in that it contains the antenna complex, reaction center, and electron-transfer chain all within the same protein. For a recent review on PSI physiology and function, we refer the reader to refs 2, 3, and 4.

A high-resolution atomic structure was recently obtained for PSI from the cyanobacterium *Synechococcus (S.) elongatus*.[5] The structure exhibits an aggregate of 96 chlorophyll molecules, including the special pair, P700, at which the primary charge separation takes place. This finding opens up the opportunity to study in detail the light-harvesting function of PSI, that is, one can computationally examine the light-harvesting pathway from initial absorption of a photon to the transfer of electrons by the special pair. In the past, a similar leap in structural information on the peripheral light-harvesting complexes LH1 and LH2 of purple bacteria resulted in the photosynthetic unit of purple bacteria being the best understood antenna complex today.[6−10]

It is of interest to compare the structure and function of PSI to the photosynthetic unit of purple bacteria. Both systems contain on the order of 100 chromophores per reaction center. In purple bacteria, these chromophores are organized in highly symmetric ring-like structures.[11−13] In contrast, the chlorophyll aggregate in PSI forms a rather random array surrounding the reaction center (see Figure 1), the only hint of order being a pseudo-C_2 symmetry apparent in the structure.

Purple bacteria have the oldest known photosynthetic apparatus, while cyanobacteria and their relatives are evolutionarily more recent.[14,15] It is of interest to compare the light-harvesting systems of these lifeforms and to elucidate the drive toward a more efficient system in the more recently developed light-harvesting complexes.

A related issue is whether the peculiar arrangement of chlorophylls found in the reported structure is essential for the functioning of PSI or whether the system can be described successfully assuming some degree of randomness. For example, is every single chlorophyll essential for the proper functioning

* To whom correspondence should be addressed. kschulte@ks.uiuc.edu.
[†] Beckman Institute, University of Illinois at Urbana-Champaign.
[‡] Department of Physics, University of Illinois at Urbana-Champaign.
[§] Virginia Polytechnic Institute and State University.
[#] Technische Universität Berlin.
[⊥] Arizona State University.

10.1021/jp020708v CCC: $22.00
Published on Web 07/18/2002

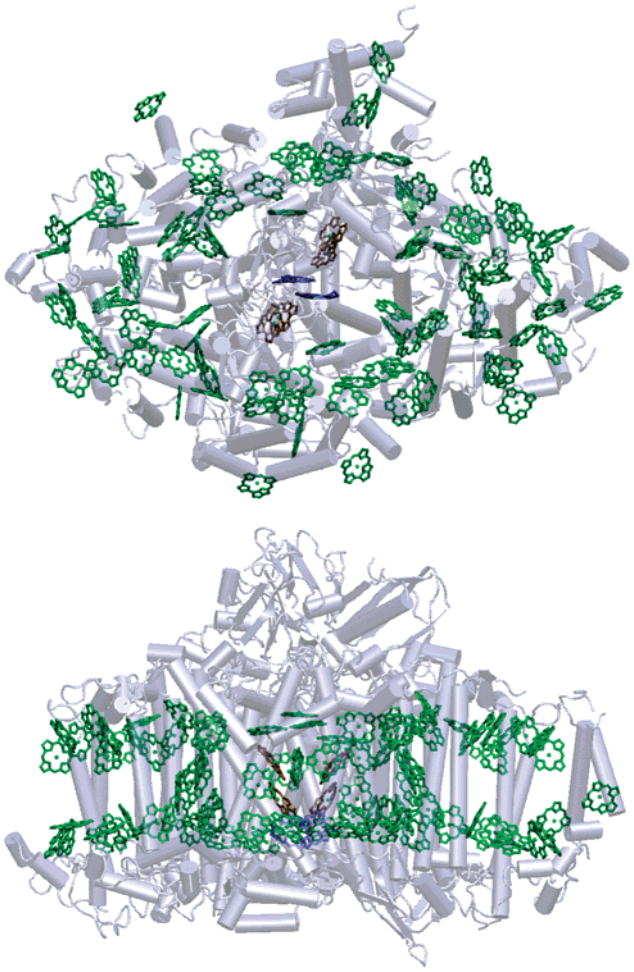

Figure 1. Photosystem I of the cyanobacterium *Synechococcus elongatus* and its 96 chlorophylls. The special pair, P700, is shown in blue. The remaining four reaction center chlorophylls are shown in red. For clarity, neither the chlorophyll tails nor the other cofactors are shown. The chlorophyll pool surrounding the reaction center displays a pseudo-C_2 symmetry. The figure was produced with VMD.[22]

of the system? This question also constitutes a modeling challenge. Because of its circular symmetry and repetitive elements, a purple bacterial light-harvesting complex can be modeled with only a few physical parameters describing chlorophyll site energies and electronic couplings.[10,16,17] PSI, on the other hand, features 96 chlorophylls that show few regularities and seemingly require a large number of parameters for their description.

There are two possible ways to approach the complexity of the chlorophyll aggregate in PSI. In one approach, typically taken in chemistry, one strives for an ever increasing accuracy in a model through a large number of specific parameters. This approach implies that the specific properties of every one of the 96 chlorophylls in PSI matter. In another approach, typically taken in physics, one identifies a minimal set of characteristics, for example, average properties of the 96 chlorophylls, relevant for the description of function and observed spectra.

The most relevant functional property of PSI is its high efficiency in using excitation energy for charge separation in the reaction center despite thermal disorder and ever present internal damage. One seeks to know how *robust* PSI is against perturbations such as "pruning" or "bleaching" of individual chlorophylls or changes in the protein that affect chlorophyll site energies. Robustness in biology is not a new concept. The issue was addressed earlier in refs 18 and 19 and, recently, in the study of biochemical networks involved in bacterial chemotaxis.[20,21] These studies suggest that biological networks exhibit a high degree of insensitivity to fine-tuning of physical parameters.

Another issue of interest is the *optimality* of the design of the chlorophyll aggregate in PSI. Is it possible to rearrange or reorient the pigments in PSI to achieve a better quantum yield or did evolution establish an optimal arrangement? This is likely easier to answer in silico than in vivo.

While the issues of robustness and optimality can be addressed well by the physicists' approach, details of the low-temperature excitation transfer dynamics and spectral features are likely better studied by the chemists' approach. The longest wavelength features of the spectrum attributed to so-called "red chlorophylls" are an example of this. Red chlorophylls are responsible for broadening the absorption profile of PSI, but their role is not fully understood. For a review, we refer the reader to ref 2.

To answer the questions raised above, we study ensembles of various chlorophyll arrangements. This permits us to investigate the dependence of the light-harvesting function of PSI in detailed or coarse descriptions, as well as the robustness and optimality of the system. For this purpose, we use the high-resolution structure reported in ref 5 as a starting point to describe the spectral and excitation transfer characteristics of PSI. The structure reveals the relative orientation of chlorophyll molecules, which makes it possible to construct an effective Hamiltonian for the chlorophyll aggregate. The resulting quantum yield for charge separation and the average excitation lifetime is determined on the basis of this Hamiltonian.

We also investigate the excitation transfer dynamics that results after the absorption of a photon by PSI. Besides determining the overall lifetime of an excitation and the quantum yield (the probability that photon absorption leads to electron transfer from the special pair), one wishes to know how excitation migrating through PSI repeatedly reaches and escapes the special pair, that is, engages in sojourns from the special pair into the chlorophyll pool. We suggest a kinetic expansion method, the sojourn expansion, to account for the outlined excitation migration in a light-harvesting complex.

The organization of this paper is as follows: In the next section, we introduce the effective Hamiltonian for the chlorophyll aggregate of PSI. Section 3 utilizes this Hamiltonian to discuss candidates for the red chlorophyll states. In section 4, we discuss the effect of thermal disorder on the spectral properties of PSI in terms of random matrix theory. In section 5, we introduce the general theoretical framework for the study of excitation transfer dynamics, including the sojourn expansion, and apply it to PSI. The robustness of the efficiency of the system is investigated under the effects of the fluctuations in chlorophyll site energies and the pruning of individual chlorophylls. In section 6, we examine the optimality of the arrangement of chlorophylls in PSI. Section 7 contains a general discussion and our conclusions. In an appendix, we summarize our method to compute interchlorophyll couplings.

2. Effective Hamiltonian for Chlorophyll Aggregate

In this section, we construct an effective Hamiltonian for the aggregate of chlorophyll molecules in PSI defined in a basis of single chlorophyll excitations. Isolated cyanobacterial PSI is known to exist in vivo mostly as a trimer.[5] In this paper, we will examine the behavior of the monomeric complex. Of the 96 chlorophylls present in PSI, 95 are chlorophyll *a* molecules and one of the special pair chlorophylls is a chlorophyll *a*′. For

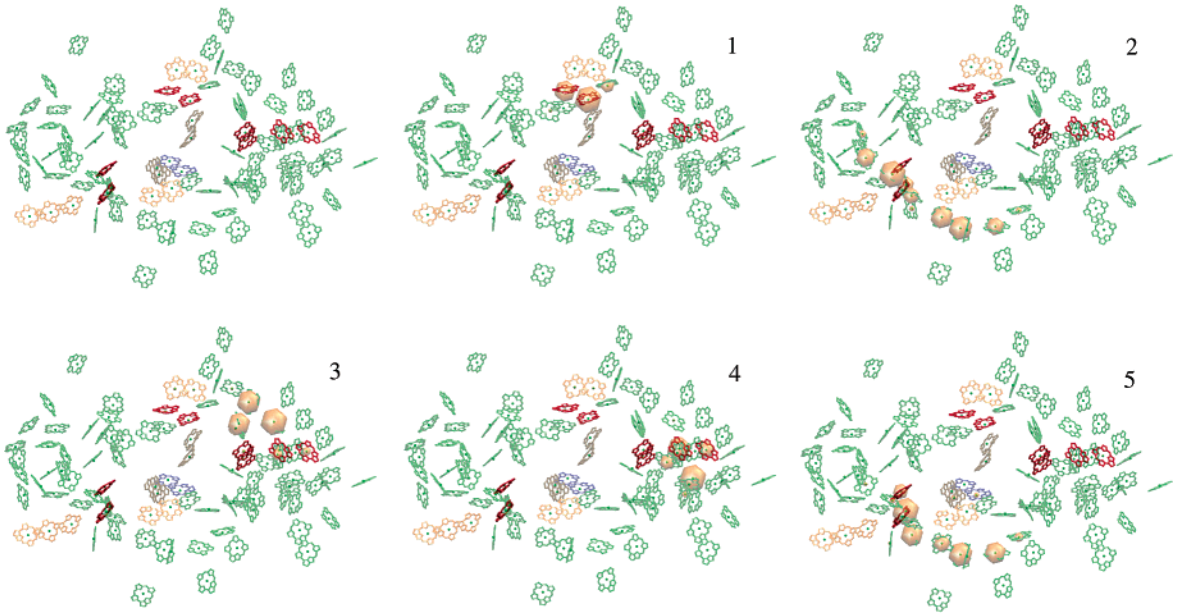

Figure 2. Excitonic (de)localization in PSI. The first five eigenstates of the effective Hamiltonian with full Coulomb couplings and identical site energies are shown. The radius of the sphere around a chlorophyll is proportional to its occupation probability in the respective state. Excitons are delocalized typically over no more than a few chlorophylls. The figure was produced with VMD.[22]

computational simplicity, we will assume herein that all chlorophylls are of chlorophyll *a* type.

The lowest excited state of a chlorophyll molecule is the Q_y state.[23] A set of basis states for an effective Hamiltonian is then given by

$$|i\rangle = |\phi_1\phi_2...\phi_i^*...\phi_N\rangle, \quad i = 1, 2, ..., N \tag{1}$$

in which the *i*th chlorophyll is Q_y-excited, all of the other chlorophylls being in their ground states. The total number of chlorophylls is $N = 96$. By using this basis, an effective Hamiltonian can be written as

$$H_0 = \begin{pmatrix} \epsilon_1 & W_{12} & W_{13} & \cdots & W_{1N} \\ W_{21} & \epsilon_2 & W_{23} & \cdots & W_{2N} \\ \cdots & \cdots & \cdots & \cdots & \cdots \\ W_{N1} & W_{N2} & W_{N3} & \cdots & \epsilon_N \end{pmatrix} \tag{2}$$

Here, ϵ_i denotes the chlorophyll site energy for the Q_y state of the *i*th chlorophyll, which needs to be determined later, and W_{ij} denotes the coupling between the *i*th and the *j*th chlorophylls.

The electronic coupling, W_{ij}, between excited states of two chlorophyll molecules has two contributions,

$$W_{ij} = W_{ij}^{c} + W_{ij}^{ex} \tag{3}$$

where W_{ij}^{c} corresponds to a direct Coulomb term[24] and W_{ij}^{ex} corresponds to an electron exchange term.[25] In PSI, almost all of the chlorophylls are at a Mg−Mg distance of greater than 7 Å, a range in which Coulomb interaction dominates;[26] therefore, we keep only the contribution of the direct Coulomb term, W_{ij}^{c}, in the remainder of the paper.

The electronic couplings due to the direct Coulomb interaction are calculated through two approaches. In the first (approximate) approach, the couplings are determined assuming a dipole−dipole interaction between transition dipole moments of the chlorophyll Q_y states. In this approximation, the couplings are given by (see, for example, ref 26)

$$W_{ij} = C\left(\frac{\mathbf{d}_i\cdot\mathbf{d}_j}{r_{ij}^{3}} - \frac{3(\mathbf{r}_{ij}\cdot\mathbf{d}_i)(\mathbf{r}_{ij}\cdot\mathbf{d}_j)}{r_{ij}^{5}}\right) \tag{4}$$

where $\mathbf{d}_i$ are unit vectors along transition dipole moments from the ground state to the Q_y state of the *i*th chlorophyll, and $\mathbf{r}_{ij}$ is the vector connecting the Mg atoms of chlorophylls *i* and *j*; the transition dipole moments for the Q_y state are taken to be along the vector connecting the N_B and N_D atoms. The latter assumption is seen to be valid by comparing the transition dipole moment unit vectors thus computed to the ones obtained in the course of the full Coulomb semiempirical method introduced below. The atomic positions are taken from crystallographic data.[5] The parameter $C = 116\,000$ Å^3 cm^{-1} in eq 4 is determined by enforcing asymptotic agreement at large distances with the full Coulomb couplings introduced below.[26] Full Coulomb couplings in turn are fixed by the oscillator strength of the Q_y transition, which is taken to be 23 D^2.[27] Because the transition dipole moment vectors are computed simply from geometry, application of eq (4) has a low computational cost. Naturally, the dipolar approximation becomes more accurate, when the distance between the chlorophylls is larger.

The second approach, following ref 26, computes electronic couplings using a semiempirical Pariser−Parr−Pople (PPP) Hamiltonian as utilized in refs 26 and 28. In this approach, the contribution of all orders of multipoles are included, that is, not only the dipole−dipole contribution. Therefore, we will refer to this description as the full Coulomb (FC) approach. The details of this approach are outlined in the appendix.

In Figure 2 are illustrated the first five eigenstates of the effective Hamiltonian (eq 2) with full Coulomb couplings and identical site energies. Excitons are localized typically only over a few chlorophylls, in some cases coinciding with strongly coupled pairs.

3. Red Chlorophyll Candidates for Photosystem I

A number of chlorophyll molecules in PSI of *S. elongatus* are known to absorb light at longer wavelengths than the special pair P700. The number of these "red chlorophylls" is suggested to be between seven and eleven.[29,30] In ref 30, individual

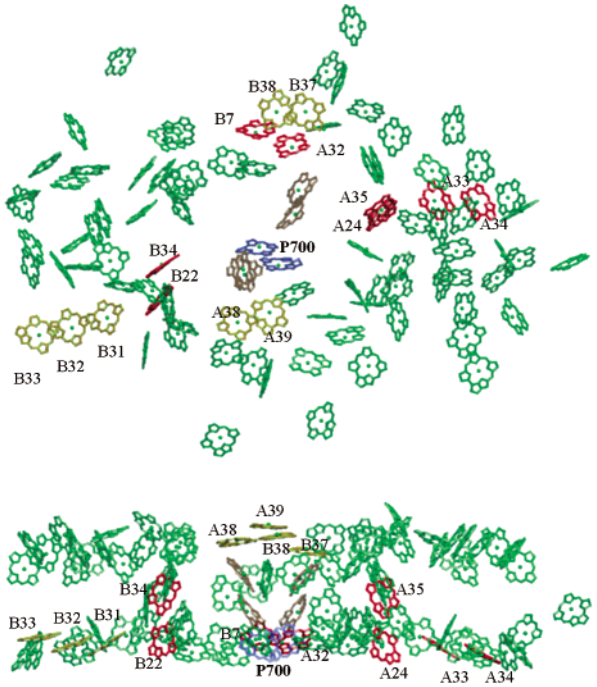

Figure 3. Red chlorophyll candidates. Chlorophylls suggested to be engaged in red absorption are highlighted in red. Red chlorophyll candidates are chosen to be the four chlorophyll pairs that exhibit the strongest couplings in the full Coulomb description, as well as a higher oscillator strength in the lower-lying excitonic state. In yellow are shown chlorophyll pairs with strong couplings in the dipolar approximation that are suggested *not* to be responsible for the red absorption in the full Coulomb description (see also text, Table 1 and Figure 4). The figure was produced with VMD.[22]

absorption peaks for the red chlorophyll states were observed for 4 K at wavelengths of 708, 715, and 719 nm. Among possible causes for this red shift in the absorption peak of these chlorophylls are the effect of the local protein environment on the site energies and the effect of excitonic splitting due to a strong coupling between pairs of chlorophylls.

In ref 5, candidates for the red chlorophylls were suggested on the basis of the orientation of chlorophylls and the assumption of a strong excitonic splitting as the cause of the spectral red shift. In ref 30, a match between these candidates and the experimentally resolved red absorption peaks were suggested. In this section, we extend this discussion by comparing the dipolar couplings with the corresponding full Coulomb couplings. In ref 5, a trimer (B31−B32−B33) and three dimers (A32−B7, B37−B38, and A38−A39) of chlorophylls were given as red chlorophyll candidates (see Figure 3; nomenclature of ref 5 is used for naming chlorophylls). Indeed in the framework of the dipolar couplings, these chlorophylls form the strongest coupled pairs. However, in the framework of the full Coulomb couplings, a different picture emerges. This may not be surprising because the two approaches tend to disagree over short distances, such as the interchlorophyll distances within strongly coupled pairs.

In the full Coulomb description, the couplings of the chlorophyll pairs in the trimer B31−B32−B33 are significantly (more than a factor 3) smaller than their corresponding dipolar couplings. Because there are chlorophyll pairs with much stronger couplings in PSI, the trimer loses its position as a red chlorophyll candidate in the full Coulomb picture.

Furthermore, a strong coupling is not enough to cause a red shift in the absorption spectrum. Viewed as a two-state system, a chlorophyll pair will have one higher-energy excitonic state and one lower-energy excitonic state, each with a certain oscillator strength. A red shift can be associated only with a case in which the lower-energy excitonic state has a higher oscillator strength than the higher-energy excitonic state. Otherwise, there needs to be a significant shift in the chlorophyll site energies due to the protein environment to account for the red shift. It turns out that the two strongest coupled pairs, B37−B38 and A38−A39, have most of their oscillator strength in the higher-energy state. Therefore, we leave them out of the list of red chlorophyll candidates.

TABLE 1: Key Chlorophyll Pairs in PSI and Their Couplings[a]

chlorophyll pair	$\|H_{ij}\|$ (FC)[b]	$\|H_{ij}\|$ (DP)[c]	O_{lo}/O_{hi}[d]
B37−B38	179	242	0.225
A38−A39	162	199	0.171
A32−B7	**161**	**255**	**10.6**
A33−A34	**153**	**193**	**14.3**
A24−A35	**131**	**88.6**	**3.69**
B22−B34	**127**	**92.6**	**3.50**
ecA1−ecB1[e]	(47.6)	272	0.31
B31−B32	(88.8)	301	191
B32−B33	(55.5)	276	75.9

[a] Pairs shown in boldface are the suggested red chlorophyll candidates according to the excitonic splittings computed in the full Coulomb picture (see text for details). [b] Full Coulomb couplings, cm^{-1}. The parentheses around the full Coulomb couplings for the special pair and the trimer B31−B32−B33 indicate that these chlorophyll groups might have to be treated as supermolecules, making the full Coulomb description inaccurate (see text and Figure 4). [c] Dipolar couplings, cm^{-1}. Note that the dipolar approximation generally overestimates the value of the coupling at short distances. [d] Ratio of oscillator strengths for the lower and higher excitonic states for full Coulomb couplings. [e] The special pair, P700.

Four pairs of chlorophylls, which have the strongest couplings, as well as the higher oscillator strength in the lower-lying state, are suggested as red chlorophyll candidates (highlighted in Table 1 and Figure 3). A match between the observed red absorption peaks and the suggested candidates cannot be done reliably without knowledge of the site energies. However, matching the furthest red shift with the strongest coupling, we tentatively suggest that A32−B7 is responsible for the 719 nm absorption peak, A33−A34 and A24−A35 for the 715 nm peak, and B22−B34 for the 708 nm peak.

It must be noted that excitonic splitting alone cannot be the only cause for observed red shifts. For example, in the case of two identical chlorophylls that have their Q_y absorption peaks at 675 nm, a coupling of about 900 cm^{-1} would be needed to place the lower-energy excitonic state at 719 nm. This suggests that the red chlorophyll states are caused by the contribution of both excitonic splitting and site energy shifts due to the local protein environment. Furthermore, any isolated chlorophyll may contribute to the red chlorophyll band of the PSI spectrum solely because of its site energy shift, a possibility that is totally neglected in our present picture.

The trimer of chlorophylls, B31−B32−B33, deserves a closer inspection than that presented thus far. As seen in Figure 4, the atomic structure indicates that the three chlorophylls are connected to each other by water molecules, suggesting that they might have to be treated computationally as a supermolecule. In regard to the possible failure of our description, we note that the histidine residue coordinating chlorophylls B31−B32−B33 is absent in *Synechocystis*, which exhibits a weaker long wavelength absorption band. Indeed, the close packing of chlorophylls B31−B32−B33 is reminiscent of J-aggregates,[31] which are known to have red-shifted spectra compared to the spectra of their building blocks. We may suggest, hence, that

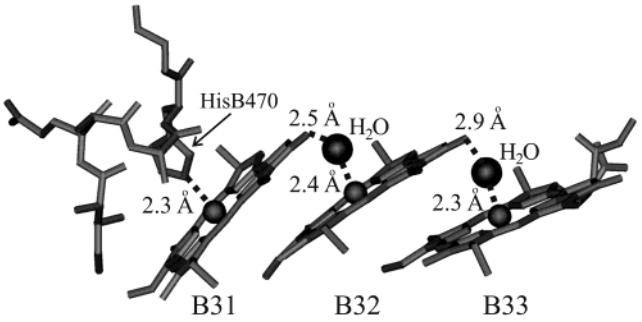

Figure 4. Chlorophyll trimer B31−B32−B33. Shown are these three closely spaced chlorophylls connected by two water molecules and coordinated by a histidine residue. The structure suggests that the trimer be described as a supermolecule. The figure was produced with VMD.[22]

the chlorophylls B31−B32−B33 may yet be responsible for red absorption, despite the weak couplings emerging from our description.

4. Effect of Thermal Disorder on Spectral Properties

Spectral properties and excitation transfer dynamics of a photosynthetic system are two complementary sources of information. Both are determined by the Hamiltonian describing the system. However, the spectral properties are influenced more by chlorophyll site energies, that is, the diagonal entries of the effective Hamiltonian, whereas the excitation transfer dynamics more directly reflects the role of interchlorophyll couplings.

A reconstruction of the (low-temperature) absorption spectrum from the Hamiltonian is not possible without a knowledge of the site energies. This is seen, for example, in the much smaller seven chlorophyll system of the FMO complex.[32] Similarly, the inverse problem of using the spectrum to reconstruct the site energies (assuming the couplings are known) is ill posed, because with as many parameters as the number of chlorophylls in the system one cannot unambiguously assign the site energies. Indeed it is a very important test for any calculation of the chlorophyll site energies to faithfully reproduce the experimentally observed absorption spectrum, especially at low temperatures.

Nevertheless, spectral data can provide valuable information on the general distribution of chlorophyll site energies if not on individual sites. Therefore, we study the spectral properties of PSI in the light of the effective Hamiltonian introduced in section 2, before we proceed with a detailed discussion of excitation transfer dynamics.

4.1. Random Matrix Theory as a Description of Thermal Disorder. Both the spectral features and the excitation transfer dynamics in a photosynthetic system need to be described in the presence of strong thermal disorder. Standard zero-temperature quantum theory remains inadequate in this respect. Below, we present a method based on random matrix theory[33−35] to study static disorder in a system described by an effective Hamiltonian, such as the one given in section 2. For a more detailed account of the application of random matrix theory to the description of static disorder in photosynthetic systems, the reader is referred to ref 36. For a discussion of dynamic disorder in a light-harvesting complex, the reader is referred to refs 37 and 38.

We consider an ensemble of Hamiltonians that describes a set of photosynthetic systems in thermal equilibrium. In contrast to a canonical ensemble from statistical mechanics, of which the members are points in the phase space of one Hamiltonian, we consider an ensemble of Hamiltonians each of which represents another copy of the photosynthetic system in question. We will be interested in spectral properties as averaged over this ensemble.

For a description of this ensemble, we employ the sum of the noise-free effective Hamiltonian, H_0, based on the crystal structure, and a random part, $\mathbf{R}$, representing thermal fluctuations

$$H = H_0 + \mathbf{R} \tag{5}$$

Here, the matrix $\mathbf{R}$ is drawn from a certain probability distribution, $P(\mathbf{R})$, representing the effects of thermal disorder. All relevant spectral quantities are defined in terms of an ensemble average over the random part, $\mathbf{R}$, with respect to the weight function, $P(\mathbf{R})$.

The density of states and the directionally averaged absorption spectrum for eq 5 are defined by

$$\rho(\omega) = \langle \sum_{i=1}^{N} \delta(\omega - E_i) \rangle \tag{6}$$

$$\alpha(\omega) = \frac{4\pi^2 \omega n}{3c} \langle \sum_i |\mathbf{D}_i^2| \delta(\omega - E_i) \rangle \tag{7}$$

where $\langle ... \rangle \equiv \int \mathrm{d}[\mathbf{R}]\, P(\mathbf{R}) ...$ and E_i are the eigenvalues of $H = H_0 + \mathbf{R}$. The transition dipole moments for eigenstates, $\mathbf{D}_i = \sum_m c_i(m)\mathbf{d}_m$, are given in terms of the transition dipole moment unit vectors of individual sites, $\mathbf{d}_m$, and the expansion coefficients, $c_i(m)$, of eigenstates.

These definitions for the average spectral behavior are superior to the "Gaussians on sticks" approach sometimes utilized, where Gaussian envelopes are put around the eigenvalues of H_0 to reconstruct the spectrum. Especially in cases in which there is a significant overlap between the envelopes of multiple eigenvalues, the average spectral properties are seen to deviate significantly. As an extreme example, one can consider a case of N degenerate eigenvalues.[34] In this case, a sum of Gaussian envelopes gives another Gaussian with the same width, whereas the width of the average spectrum should be proportional to $\sqrt{N}$.

The nature of the probability distribution, $P(\mathbf{R})$, as a function of temperature is not easy to determine. However, studies in random matrix theory have shown that many average spectral features are largely independent of the exact shape of $P(\mathbf{R})$ and instead depend mainly on its width.[35] This kind of independence from the specific probability distribution is akin to the central limit theorem and is known as random matrix universality. This universality allows one to make simplifying assumptions on the nature of $P(\mathbf{R})$.[35]

Although most results on random matrix universality are based on the limit at which the matrix size becomes large, remarkable spectral similarity persists even for mesoscopically sized ensembles. In an earlier investigation, we have applied random matrix universality to the peripheral light-harvesting complex LH2 of purple bacteria,[36] which has 16 strongly coupled bacteriochlorophylls. It was seen that, when the width of the disorder term, $P(\mathbf{R})$, is taken into account the average density of states and the absorption spectrum are rather insensitive to the changes of $P(\mathbf{R})$. Analytical formulas for the density of states at finite temperature as a function of the zero-temperature spectrum were derived for a simple form of $P(\mathbf{R})$ in ref 36.

In the following, we take the probability distribution, $P(\mathbf{R})$, to describe diagonal disorder

$$P_{\mathrm{diag}}(\mathbf{R}) = N_{\mathrm{diag}} \prod_i \exp\left(-\frac{1}{2\nu_{\mathrm{diag}}^2} R_{ii}^2\right) \prod_{i \neq j} \delta(R_{ij}) \quad (8)$$

For the width of the distribution (eq 8), we take $\nu_{\mathrm{diag}} = 70\ \mathrm{cm}^{-1}$ at 4 K.[39,40] A similar description has been used in ref 10 for the light-harvesting system of purple bacteria. We use the parameter ν_{diag} to numerically evaluate the absorption spectrum as defined in eq 7. In Figure 5 is shown the absorption spectrum at 4 K based on the effective Hamiltonian with full Coulomb couplings and homogeneous site energies corresponding to 675 nm. When the red chlorophyll band of the spectrum is ignored, a width for the bulk of about 230 cm^{-1} (corresponding to a full width at half-maximum of 550 cm^{-1}) at 4 K is reported in ref 30. However, the width for the 4 K spectrum in Figure 5 measures only about 140 cm^{-1}. The mismatch can be attributed to our neglect of the site energy heterogeneity.

Though it is not possible to reconstruct the chlorophyll site energies from the spectrum, one can obtain an estimate on the width of the distribution of site energies. To accomplish this, we will ignore for the moment the red chlorophyll band of the spectrum and instead concentrate on the main peak as given in ref 30. The width of the absorption spectrum for the actual (inhomogeneous) site energies, W_{inhom}, the width of the absorption spectrum for the homogeneous site energies, W_{hom}, and the width of the distribution of site energies (heterogeneity), W_ϵ, are approximately related to each other by

$$W_{\mathrm{inhom}}^2 = W_{\mathrm{hom}}^2 + W_\epsilon^2 \quad (9)$$

As discussed above, assuming $W_{\mathrm{inhom}} = 230\ \mathrm{cm}^{-1}$ and $W_{\mathrm{hom}} = 140\ \mathrm{cm}^{-1}$ results in a site energy distribution width of about $W_\epsilon = 180\ \mathrm{cm}^{-1}$ (fwhm of 430 cm^{-1}). The validity of this assertion can be numerically verified by generating an ensemble of Hamiltonians with the same full Coulomb couplings but with random site energies for the given value of W_ϵ. This value will be utilized later in the discussion of excitation transfer dynamics.

5. Excitation Transfer Dynamics in Photosystem I

In this section, we construct the excitation transfer rates between chlorophylls using Förster theory.[24] We will follow the methodology suggested in ref 41. The excitation transfer rate from chlorophyll i to chlorophyll j is[24,25]

$$T_{ij} = \frac{2\pi}{\hbar} |H_{ij}|^2 J_{ij}, \quad J_{ij} = \int S_i^{\mathrm{D}}(E) S_j^{\mathrm{A}}(E)\, \mathrm{d}E \quad (10)$$

where H_{ij} is the coupling between the chlorophylls and J_{ij} is the spectral overlap between the emission spectrum, $S_i^{\mathrm{D}}(E)$, of the donor chlorophyll i and the absorption spectrum, $S_j^{\mathrm{A}}(E)$, of the acceptor chlorophyll j. Following refs 41 and 42, we approximate these spectra by Gaussians

$$S_i^{\mathrm{D}}(E) = \frac{1}{\sqrt{2\pi}\nu} \exp\left(-\frac{(E_i - S - E)^2}{2\nu^2}\right)$$

$$S_j^{\mathrm{A}}(E) = \frac{1}{\sqrt{2\pi}\nu} \exp\left(-\frac{(E_j - E)^2}{2\nu^2}\right) \quad (11)$$

where E_i and E_j are the absorption peaks for the chlorophylls and S is the Stokes shift. We take the Stokes shift to be equal to 160 cm^{-1} at room temperature[23] and 20 cm^{-1} at 4 K.[43] We have assumed identical widths for the emission and absorption spectra of 240 cm^{-1} at room temperature.[23] In the case of identical site energies, rates for forward transfer and back transfer are equal, $T_{ij} = T_{ji}$, but this is not the case when the site energies differ. The network of excitation transfer rates between chlorophylls of PSI for identical site energies is shown in Figure 6 for both the full Coulomb and dipolar Hamiltonians.

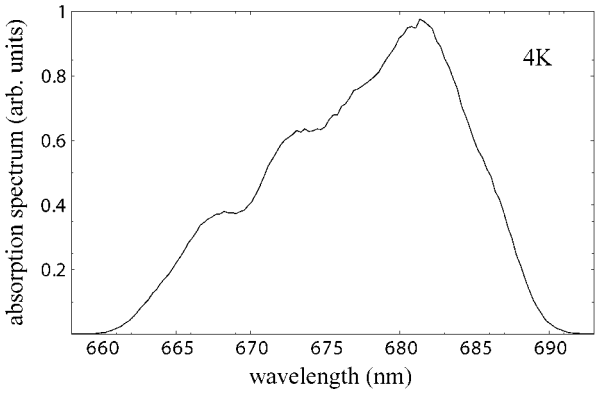

Figure 5. Absorption spectrum. Shown is the low-temperature (4 K) spectrum for an effective Hamiltonian with full Coulomb couplings and homogeneous site energies (675 nm). The spectrum is generated for an ensemble with diagonal disorder corresponding to 70 cm^{-1}. A comparison of the width of this spectrum with that of the experimental absorption spectrum[30] allows the prediction of the heterogeneity in the site energies.

The largest transfer rate away from a given chlorophyll suggests the average excitation lifetime at that chlorophyll. Figure 7 shows the largest excitation transfer rates for all 96 chlorophylls. It can be seen that these rates correspond to an average largest transfer rate between chlorophylls of about 11 ps^{-1}.

Using the transfer rates between the chlorophylls, we can construct a master equation for the rate of change of probabilities, $p_i(t)$, describing the likelihood that the chlorophyll i is electronically excited at time t. The corresponding rate equation is

$$\frac{\mathrm{d}}{\mathrm{d}t} p_i(t) = \sum_j K_{ij} p_j(t) \quad (12)$$

$$K_{ij} = T_{ji} - \delta_{ij}\left(\sum_k T_{ik} + k_{\mathrm{diss}} + \delta_{i,\mathrm{P700}} k_{\mathrm{CS}}\right) \quad (13)$$

where k_{diss} denotes the dissipation (internal conversion) rate, which is assumed to be uniform among the chlorophylls, k_{CS} denotes the charge separation rate at the special pair P700, and $\delta_{i,\mathrm{P700}}$ is equal to 1 when i is one of the two chlorophylls in the special pair and zero otherwise. The dissipation and charge separation rates are not known to great accuracy. Inspired by the purple bacterial light-harvesting systems,[41] we assume a dissipation rate of $k_{\mathrm{diss}} = (1\ \mathrm{ns})^{-1}$. The charge separation rate at P700 is observed to be between 1 ps^{-1} and 3 ps^{-1}.[44−46] In the following, we will assume a charge separation rate of $k_{\mathrm{CS}} = (1.5\ \mathrm{ps})^{-1}$.

Given an initial distribution, $p_i(0)$, the formal solution to eq (12) can be written

$$|p(t)\rangle = \exp(Kt)\, |p(0)\rangle \quad (14)$$

Using this expression, we can give explicit formulas for the average excitation lifetime, the quantum yield, and overall dissipation rate.[41]

Let us define a uniform (nonnormalized) state, $|\mathbf{1}\rangle \equiv \sum_i |i\rangle$, describing equally likely occupation probabilities for all chlorophylls. If we assume this uniform distribution for the initial

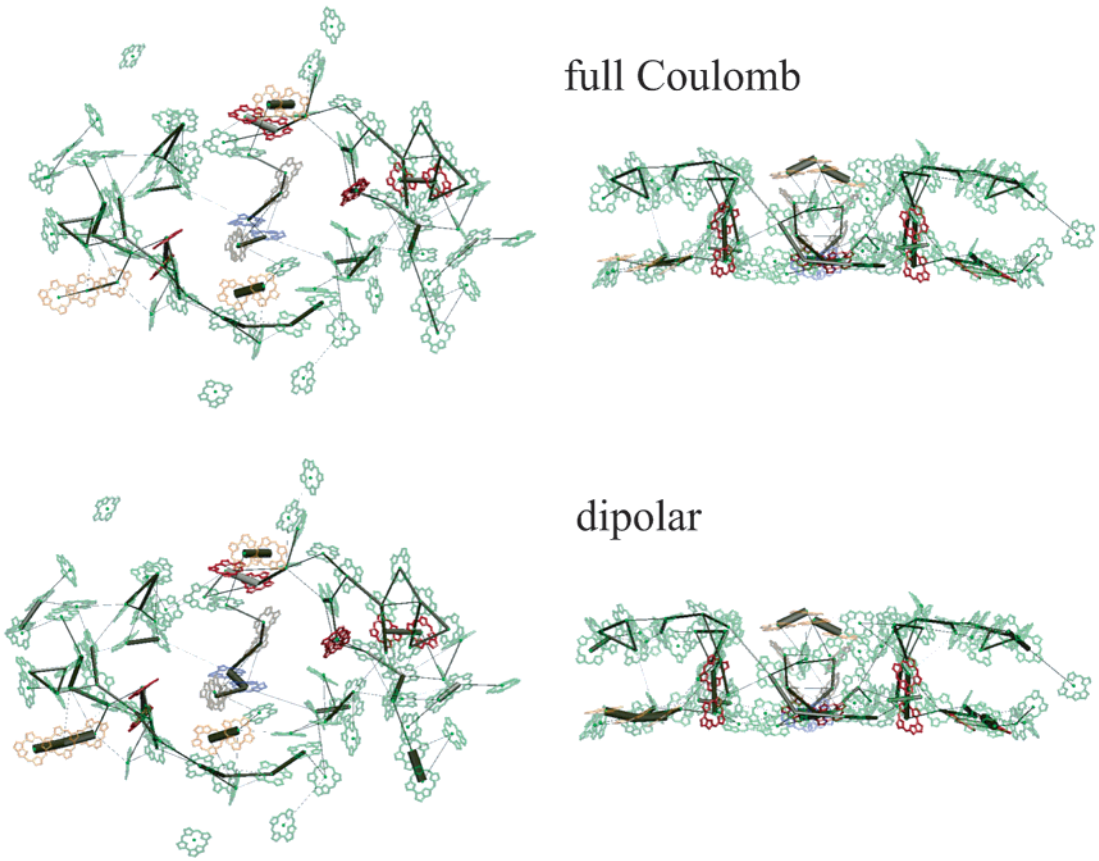

Figure 6. Network of excitation transfer pathways in PSI. The networks at room temperature for full Coulomb couplings (top) and dipolar couplings (bottom) are shown. The thickness of bonds connecting chlorophylls are proportional to the transfer rates between them. Only the 130 largest transfer rates are presented. The transfer rates are computed for a system with identical site energies at room temperature. The figure was produced with VMD.[22]

state, that is, $|p(0)\rangle = N^{-1}|\mathbf{1}\rangle$, then the average excitation lifetime, τ, the quantum yield, q, and the overall dissipation probability, d, are all given in terms of similar expressions[41]

$$\tau = -\frac{1}{N}\langle \mathbf{1}|K^{-1}|\mathbf{1}\rangle \tag{15}$$

$$q = -\frac{1}{N}k_{\mathrm{CS}}\langle \mathrm{P700}|K^{-1}|\mathbf{1}\rangle = 1 - d \tag{16}$$

$$d = -\frac{1}{N}k_{\mathrm{diss}}\langle \mathbf{1}|K^{-1}|\mathbf{1}\rangle = k_{\mathrm{diss}}\tau \tag{17}$$

where $|\mathrm{P700}\rangle \equiv \sum_i \delta_{i,\mathrm{P700}}|i\rangle$.

Average excitation lifetimes and the quantum yields for various models are provided in Table 2. The data in the first three rows are based on an effective Hamiltonian that assumes identical site energies for the two chlorophylls of the P700 pair. The site energies were chosen such that the P700 excitonic state with the highest oscillator strength coincides with the 698 nm (14 327 cm^{-1}) absorption peak at 4 K. Because one of the two P700 chlorophylls is a chlorophyll *a*′, the identical site energy assumption for the P700 is likely to be unrealistic; however, it shall be adequate for an approximate description of the excitation transfer dynamics. For full Coulomb couplings, the highest oscillator strength lies at the higher-energy excitonic state (see Table 1); because the respective coupling between the two P700 chlorophylls is 47.6 cm^{-1}, the P700 site energy is chosen to be 14 279 cm^{-1}. For dipolar couplings, the highest oscillator strength lies at the lower-energy excitonic state (the sign of the coupling is different for the two methods); the coupling between the two P700 chlorophylls is 272 cm^{-1} requiring a P700 site energy of 14 599 cm^{-1}. The site energies for the remaining chlorophylls are placed at 675 nm (14 815 cm^{-1}) unless otherwise noted.

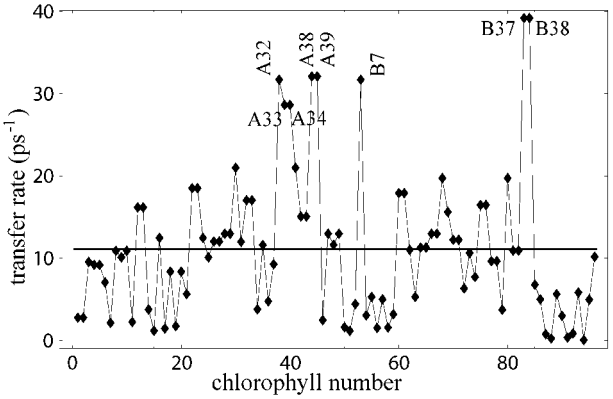

Figure 7. Largest excitation transfer rate from PSI chlorophylls. Shown are rates for all 96 PSI chlorophylls as a function of the donor chlorophyll. The horizontal line indicates the average value of 11.1 ps^{-1}. The excitation transfer rates are computed for a Hamiltonian with full Coulomb couplings and homogeneous site energies for all chlorophylls, except P700 (cf. row 1, Table 2).

The efficiency of 97.3% and the average excitation lifetime of 27.4 ps for full Coulomb couplings, given in the first row of Table 2, are in general agreement with the near unit efficiency and the 20−40 ps lifetime reported for PSI at room temperature.[2,47−51] A recent estimate of the average excitation lifetime reported for trimeric PSI in *S. elongatus* is 35.8 ps.[47] A comparison between the first and the last rows in Table 1 shows the importance of having P700 chlorophylls at a lower energy

TABLE 2: Average Excitation Lifetime and Quantum Yield

model	lifetime (ps)	quantum yield (%)
A[a]	**27.4**	**97.3**
B[b]	45.9	95.4
C[c]	**28.8**	**97.1**
D[d]	75.3	92.5

[a] Full Coulomb couplings with P700 *tuned* (see text) to the observed absorption peak and with identical site energies (675 nm) for the chlorophyll pool. [b] Dipole−dipole couplings with P700 tuned to the observed absorption peak and with identical site energies (675 nm) for the chlorophyll pool. The difference in lifetimes for models A and B are mainly due to the difference of site energy assignments for P700 for dipolar and full Coulomb models. [c] Full Coulomb couplings with P700 tuned to the observed absorption peak but with random site energies (centered around 675 nm with a width of 180 cm^{-1}) for the chlorophyll pool. Ensemble average value is given here. For more detail, see Figure 8. [d] Full Coulomb couplings with identical site energies (675 nm) for all chlorophylls, including P700.

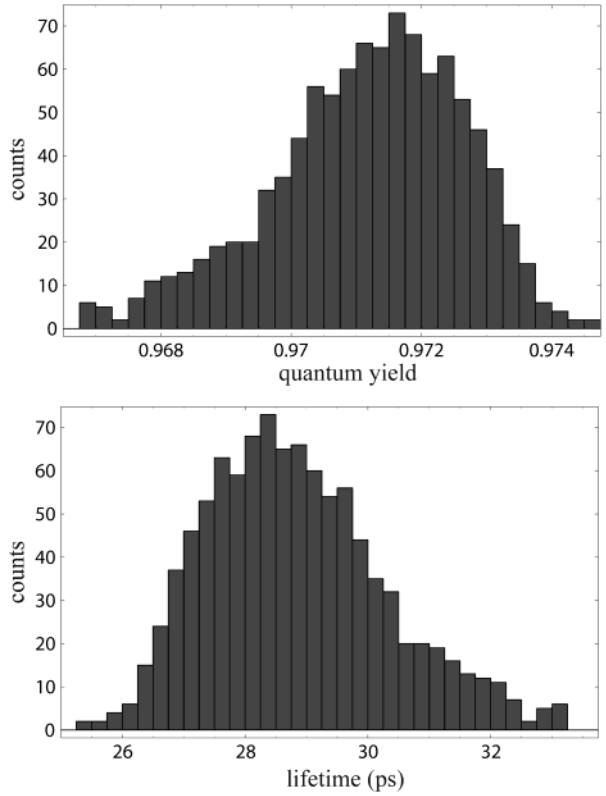

Figure 8. Effect of fluctuations of the site energies (heterogeneity) on excitation transfer dynamics. Shown are the distributions of quantum yield and lifetime at room temperature for an ensemble of effective Hamiltonians with full Coulomb couplings. The ensemble consists of systems in which P700 was tuned to the observed absorption peak and with the rest of the chlorophyll site energies chosen randomly with a width of 180 cm^{-1} around 675 nm. The histograms were generated from an ensemble of 1000 systems.

than the bulk of the chlorophylls to decrease the trapping time and to increase efficiency.

In Figure 8 is provided the distribution of quantum yield and average excitation lifetime across an ensemble of Hamiltonians with full Coulomb couplings, P700 tuned to the observed absorption peak, and all other chlorophyll site energies randomly distributed with a width of 180 cm^{-1} around 675 nm (thus the ensemble covers different realizations of heterogeneity and not static disorder). Figure 8 reveals that, at room temperature, fluctuations in the site energies (heterogeneity) have no considerable effect on efficiency. This allows us to reconstruct

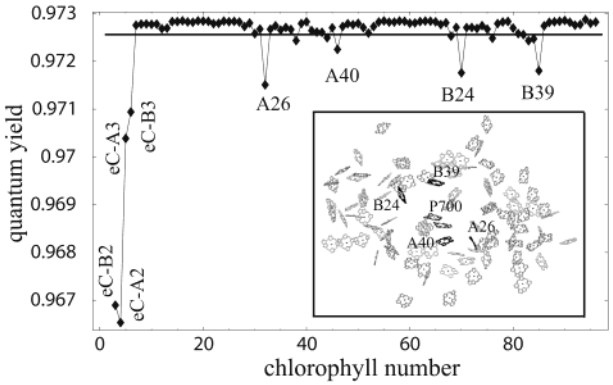

Figure 9. Quantum yield for pruned chlorophylls. Shown is the quantum yield resulting after pruning of individual chlorophylls. The chlorophylls the deletion of which has the highest impact on quantum yield are labeled. Chlorophylls (eC-xx), numbered 3 to 6, are part of the reaction center. Chlorophylls A26, A40, B24, and B39 are connecting chlorophylls situated closest to the reaction center (see inset). The horizontal line denotes the efficiency of the unperturbed system (97.25%), which is described by the effective Hamiltonian with full Coulomb couplings, identical site energies, and P700 tuned to the observed absorption spectrum (cf. row 1, Table 2).

room-temperature excitation transfer dynamics with reasonable accuracy even without detailed knowledge of the chlorophyll site energies. However, at 4 K, the line shapes of individual chlorophylls become so narrow that the spectral overlap integrals in eq 10 become unrealistically small for misplaced site energies. Also at low temperatures, the broadening of spectral line shapes due to electron−phonon couplings[30] need to be taken into account because this broadening is likely to effect the overlap integrals in the context of Förster theory. We find it impossible to construct a reliable picture of the low-temperature excitation transfer dynamics with the current data.

It is of interest to know in how far low-energy chlorophylls control the excitation transfer dynamics and trapping in PSI. In this regard, one may construct models in which the red chlorophyll candidates given in section 3 are used to refine the assignment of chlorophyll site energies. However, it must be kept in mind that an accurate assignment of an individual chlorophyll pair to an observed red chlorophyll state cannot be done reliably without a precise knowledge of site energies. It is seen that the room-temperature excitation transfer dynamics is not effected greatly by the inclusion of this extra information in a model in which all other site energies are unknown or taken to be random. Figure 8 supports this claim. As a result, we find it rather unfruitful to proliferate the multitude of models already given in Table 2. At room temperature, the role of low-energy chlorophylls appears to be simply to extend the absorption profile to longer wavelengths rather than to have a profound effect on the excitation transfer dynamics. However, at low temperatures, red chlorophylls may function as effective traps and could serve as probes to investigate the excitation transfer dynamics of PSI in detail.

5.1. Effect of Removal of Individual Chlorophylls on Excitation Transfer Dynamics. One way to probe the function of individual chlorophylls in PSI, as well as the degree of robustness in its design, is to examine the effect of the removal of chlorophylls on the efficiency of the system. To this end, we remove various chlorophylls one at a time and examine the quantum yield of the remaining system.

Figure 9 shows the quantum yield as a function of the removed chlorophyll. The two P700 chlorophylls are not removed in this study. Although the effect of the removal of the other four reaction center chlorophylls on the quantum yield

is shown, it is hard to test their effect directly, because they are also a part of the electron-transfer chain. Therefore, we will concentrate on the remaining 90 chlorophylls.

It is interesting to note that, except for the four reaction center chlorophylls, which are immediate neighbors to the P700, removal of a chlorophyll hardly has any effect on the quantum yield. In fact, for most of the chlorophylls, a deletion results in an increase in the quantum yield. This is a consequence of the relative yield being defined with respect to the remaining chlorophylls and not with respect to the unperturbed system.

Thus it is seen that, outside the reaction center, no chlorophylls play the role of a gatekeeper for excitation transfer, the removal of which would have an adverse effect on the yield. Instead, the individual chlorophylls contribute to the overall cross-section of the antenna complex. Outside the electron-transfer chain, the four chlorophylls with the highest impact on efficiency (A26, B24, B39, and A40) are the nearest neighbors of the six reaction center chlorophylls. These chlorophylls, especially A40 and B39, appear to link the antenna system to the reaction center and are therefore referred to as connecting chlorophylls. As an extreme example, one may consider the removal of all four of these chlorophylls simultaneously. Even in this case, the quantum yield reduces to only 96.85% from the value of 97.25% for the unperturbed complex with the same Hamiltonian; the average excitation lifetime increases from 27.4 to 31.5 ps upon removal. These results agree with some of the simulations reported in ref 52.

5.2. An Expansion of the Average Lifetime in Terms of Return Times to the Reaction Center. The average excitation lifetime, τ, can be expanded in terms of processes describing the initial delivery of excitation to the special pair and possible subsequent returns following detrapping. To establish such an expansion, we rewrite the excitation transfer rates (eq 12) in a form in which P700 is treated as a single excitonically coupled unit as opposed to two separate chlorophylls.

A two-state Hamiltonian for P700 is given by

$$H_{\mathrm{P700}} = \begin{pmatrix} \epsilon_1 & U_{\mathrm{P700}} \\ U_{\mathrm{P700}} & \epsilon_2 \end{pmatrix} \tag{18}$$

where ϵ_1 and ϵ_2 are the site energies for the two P700 chlorophylls and U_{P700} denotes the coupling between them. Not knowing the values of the site energies, we will assume below that $\epsilon_1 = \epsilon_2$. However, the expansion below can be readily applied to nonidentical site energies.

Let us denote the eigenvalues of the two-state system (eq 18) by E_1 and E_2 and the corresponding eigenfunctions by

$$\begin{aligned} \Psi_1^{\mathrm{P700}} &= c_{1,1}|1\rangle + c_{1,2}|2\rangle \\ \Psi_2^{\mathrm{P700}} &= c_{2,1}|1\rangle + c_{2,2}|2\rangle \end{aligned} \tag{19}$$

respectively. Then the coupling of any of the other chlorophylls, $j = 3, ..., N$, to any eigenstate, $m = 1, 2$, of P700 is

$$\tilde{H}_{mj} = \tilde{H}_{jm} = \sum_{\alpha=1}^{2} c_{m,\alpha} H_{j\alpha} \tag{20}$$

where $H_{j\alpha}$ are the elements of the original effective Hamiltonian (eq 2).

We will assume that thermal equilibration between eigenstates of P700 has been achieved before excitation transfer out of P700 occurs. This is likely to be a reasonable assumption at room temperature for full Coulomb couplings, at which $k_{\mathrm{B}}T = 209$ cm^{-1} is larger than the interchlorophyll couplings. The expansion outlined below can also be formulated for a reaction center in which multiple chlorophylls without a strong excitonic character are responsible for charge separation, making the thermal equilibration assumption invalid. However, in that case, the final formulation of the expansion cannot be written as succinctly as eq 31.

The excitation transfer from P700 to any other chlorophyll is given by a Boltzmann-weighted sum

$$\begin{aligned} \tilde{T}_{\mathrm{P700},j} &= \sum_{m=1}^{2} \tilde{T}_{mj} \\ \tilde{T}_{mj} &= \frac{2\pi}{\hbar} \frac{\mathrm{e}^{-E_m/(k_{\mathrm{B}}T)}}{\sum_{n=1}^{2} \mathrm{e}^{-E_n/(k_{\mathrm{B}}T)}} |\tilde{H}_{mj}|^2 \int S_m^{\mathrm{D}}(E) S_j^{\mathrm{A}}(E)\, \mathrm{d}E \end{aligned} \tag{21}$$

where we assume an identical line shape for the eigenstates of P700, chosen equal to the line shape of all other chlorophylls in PSI. The excitation transfer rate from another chlorophyll to P700 is

$$\tilde{T}_{j,\mathrm{P700}} = \sum_{m=1}^{2} T_{j,m} \tag{22}$$

where $T_{j,m}$ are given by eq 10, except that $m = 1, 2$ now denotes an eigenstate of P700 as given in eq 19.

A reduced $(N-1) \times (N-1)$ transfer-rate matrix, $\tilde{T}$, can be constructed using these rates. The corresponding matrix, $\tilde{K}$, that enters in eq 12 governing the kinetics of PSI is

$$\tilde{K}_{ij} = \tilde{T}_{ji} - \delta_{ij}\Big(\sum_k \tilde{T}_{ik} + k_{\mathrm{diss}} + \delta_{i,\mathrm{P700}} k_{\mathrm{CS}}\Big) \tag{23}$$

Average excitation lifetime, τ, and quantum yield of the system are defined as in eqs 15 and 16, for example,

$$\tau = -\frac{1}{N-1} \langle \mathbf{1}|\tilde{K}^{-1}|\mathbf{1}\rangle \tag{24}$$

where $|\mathbf{1}\rangle = |P700\rangle + \sum_{j=3}^{N}|j\rangle$ denotes the (nonnormalized) uniform initial state (in the basis of this reduced Hamiltonian $|P700\rangle$ denotes the vector with a one in the first column and zeroes everywhere else).

We introduce now the expansion of the average excitation lifetime. The terms that arise in this expansion are introduced and explained in Figure 10. For the purpose of this expansion, we separate from $\tilde{K}$ the operator Δ that describes detrapping

$$\begin{aligned} \tilde{K} &\equiv \kappa + \Delta \\ \Delta &\equiv \begin{pmatrix} 0 & 0 & \cdots & 0 \\ \tilde{T}_{\mathrm{P700},3} & 0 & \cdots & 0 \\ \tilde{T}_{\mathrm{P700},4} & 0 & \cdots & 0 \\ \cdots & \cdots & \cdots & \cdots \\ \tilde{T}_{P700,N} & 0 & \cdots & 0 \end{pmatrix} \end{aligned} \tag{25}$$

The inverse, $\tilde{K}^{-1}$, that enters in eq 24, can be expressed through Taylor expansion in Δ

$$\begin{aligned} \tilde{K}^{-1} &= (\kappa + \Delta)^{-1} = (\mathbf{1} + \kappa^{-1}\Delta)^{-1}\kappa^{-1} \\ &= \kappa^{-1} - \kappa^{-1}\Delta\kappa^{-1} + \kappa^{-1}\Delta\kappa^{-1}\Delta\kappa^{-1} - ... \end{aligned} \tag{26}$$

where $\mathbf{1}$ is the $(N-1) \times (N-1)$ identity matrix. The validity of this expansion can be proven by noting that the absolute value

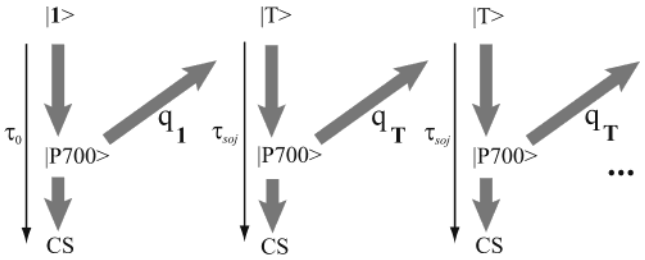

Figure 10. Processes contributing to the overall excitation lifetime. The excitation in a uniform initial state $|\mathbf{1}\rangle$ (see text) after reaching the special pair $|P700\rangle$ either causes a charge separation (CS) or, with detrapping probability q_1, returns to the surrounding chlorophylls through the transient state $|T\rangle$ (see text). From the transient state, excitation migrates through PSI to return to $|P700\rangle$ after which charge separation occurs or, again with detrapping probability q_T, the transient state $|T\rangle$ is reached once more. The process of migration, return to $|P700\rangle$, and possibly charge separation or renewed detrapping is repeated. The first usage time, τ_0, is the sum of the delivery-to-trap time starting from a uniform state, $|\mathbf{1}\rangle$, and of the charge separation time. τ_0 represents the average time that it takes for charge separation to take place if no detrapping events occur. The sojourn time, τ_{soj}, is the sum of the delivery-to-trap time starting from the transient state, $|T\rangle$, and of the charge separation time. After subtracting the charge separation time, τ_{soj} may be viewed as the return time back to P700 after a detrapping event. Dissipation processes are not shown.

of the eigenvalues of $\kappa^{-1}\Delta$ are less than one. Substituting this expansion into eq 24 results in a decomposition of the lifetime into a series

$$\tau \equiv \tau_0 + \tau_1 + \tau_2 + ... \tag{27}$$

where

$$\tau_0 = -\frac{1}{N-1}\langle \mathbf{1}|\kappa^{-1}|\mathbf{1}\rangle$$
$$\tau_1 = \frac{1}{N-1}\langle \mathbf{1}|\kappa^{-1}\Delta\kappa^{-1}|\mathbf{1}\rangle$$
$$\tau_2 = -\frac{1}{N-1}\langle \mathbf{1}|\kappa^{-1}\Delta\kappa^{-1}\Delta\kappa^{-1}|\mathbf{1}\rangle ... \tag{28}$$

One can simplify eq 28 by noting that Δ can be expressed as $\Delta = W_D|T\rangle\langle P700|$, where $W_D = \sum_{j=3}^{N} T_{P700,j}$ is the total detrapping rate from the special pair, P700, and where $|T\rangle = W_D^{-1} \sum_{j=3}^{N} T_{P700,j}|j\rangle$ is a transient state representing the occupation probabilities right after a detrapping event has occurred. Substituting Δ, thus factored, into eq 28, we can write the expansion terms for the average excitation lifetime

$$\tau_1 = q_1\tau_{soj}$$
$$\tau_2 = q_1 q_T \tau_{soj}$$
$$\tau_3 = q_1 q_T^{\,2} \tau_{soj} ... \tag{29}$$

where the defining parameters are

$$\tau_{soj} = -\langle \mathbf{1}|\kappa^{-1}|T\rangle$$
$$q_1 = -\frac{W_D}{N-1}\langle P700|\kappa^{-1}|\mathbf{1}\rangle$$
$$q_T = -W_D\langle P700|\kappa^{-1}|T\rangle \tag{30}$$

The terms appearing in eq 29 can be summed to give

TABLE 3: Characteristics of Sojourn Expansion[a]

τ	τ_0	τ_{soj}	q_1	q_T
27.6 ps	11.8 ps	4.55 ps	77.2%	77.8%

[a] The quantities given (for definition, see Figure 10 and eq 31) have been evaluated for the effective Hamiltonian with full Coulomb couplings and adjusted P700 site energies (row 1, Table 2).

$$\tau = \tau_0 + \frac{q_1}{1-q_T}\tau_{soj} \tag{31}$$

The expansion decomposes the average excitation lifetime in terms of multiple escapes and returns (sojourns) to the reaction center, and hence, we call it the sojourn expansion.

Terms arising in the sojourn expansion for an effective Hamiltonian with full Coulomb couplings (see row 1 of Table 2) are provided in Table 3. It can be seen that the time for a first delivery of excitation to P700, approximately given by τ_0, constitutes less than half of the average excitation lifetime at room temperature.

6. How Optimal is the Design of Photosystem I?

At first glance, the arrangement of chlorophylls in PSI appears to be random except for a pseudo-C_2 symmetry (see Figure 1). Especially when compared to the regular circular aggregates found in purple bacterial photosynthetic systems, this brings up the question of whether the particular arrangement of chlorophylls in PSI is optimal in some way.

Even though the fitness landscape over which a photosynthetic apparatus should be judged is many dimensional, a crude measure of optimality is given by the quantum yield of the system. Ignoring all other concerns for optimality from an evolutionary perspective, such as assembly, aggregation, and interaction with other biomolecules in the cell, we examine whether the chlorophyll aggregate in PSI can be rearranged to result in a better quantum yield.

To keep the number of parameters to be varied at a manageable level, the chlorophyll positions (as defined by their Mg atoms), as well as the chlorophyll site energies, are kept fixed. Instead, we consider an ensemble of alternate PSI's formed by random independent reorientations of constituent chlorophylls.

It is costly to repeat the semiempirical computation of full Coulomb couplings between chlorophylls for a large ensemble of chlorophyll arrangements. Therefore, we revert to dipolar couplings for this study. The ensemble in question is formed by taking the vector for the transition dipole moment at each chlorophyll and multiplying it by a randomly generated SO(3) rotation matrix, thus reorienting it. A new effective Hamiltonian is then computed using the couplings between these new transition dipole moment vectors as explained in section 2, while keeping the same site energies as before. The effective Hamiltonians thus generated are used to compute the quantum yield and the average excitation lifetime at room temperature. For this study, identical site energies (675 nm) for all chlorophylls are chosen except for P700, the site energies of which are chosen in such a way as to coincide with the observed absorption peak, as explained in section 5. Therefore, the results of this study should be compared with the original arrangement of chlorophylls given in row 2 of Table 2.

Figure 11 contains a histogram of quantum yields and average excitation lifetimes for this ensemble at room temperature. The values for the original arrangement of chlorophylls are indicated by an arrow. It is seen that the original chlorophyll arrangement

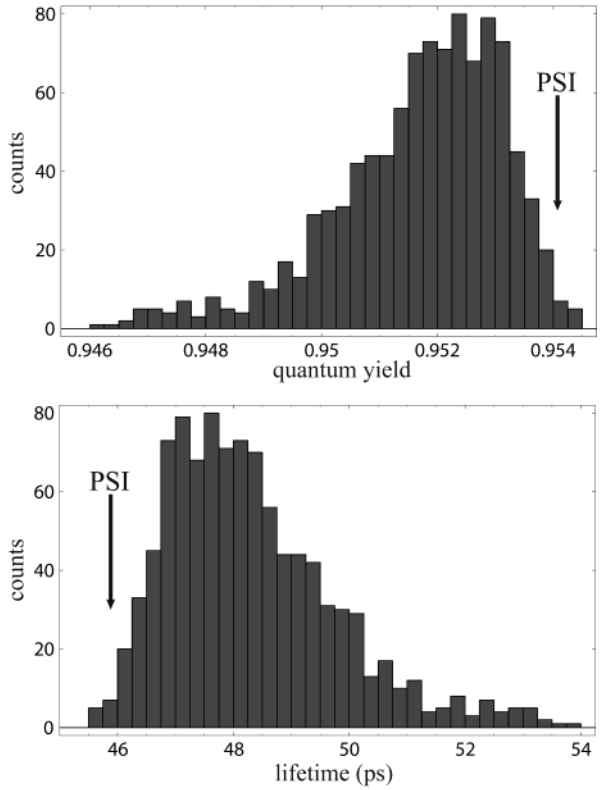

Figure 11. Optimality of PSI. The distributions of quantum yield and average excitation lifetime for an ensemble of randomly generated chlorophyll aggregates at room temperature are shown. Chlorophyll couplings are computed in the dipolar approximation to reduce computational cost. P700 site energies are tuned to the observed absorption peak and the remaining site energies are taken to be identical (675 nm). The histograms are generated from an ensemble of 1000 systems. The results for the original arrangement (cf. row 2, Table 2) of chlorophylls are indicated by an arrow.

is nearly at the top of the distribution, though a few arrangements can be found to have a better quantum yield. This does not necessarily imply, however, that the efficiency of PSI can be easily improved upon. Not only is the study of quantum yields outlined above approximate in nature, but also there is no way to accurately model the constraints that had to be satisfied over the course of the evolution of this system. Nevertheless, it is impressive to find the original chlorophyll arrangement at near-top efficiency.

The relatively small variation in the quantum yield across the ensemble seen in Figure 11 brings up the question as to whether the apparent optimality is an artifact that will disappear in a more accurate computation. This small variation is a result of the nearly 3 orders of magnitude difference between the dissipation and charge transfer rates. As an ultimate test, full Coulomb couplings need to be computed for each system in an ensemble of randomly oriented chlorophyll aggregates and the effect of individual site energies also need to be taken into account. This is beyond the scope of this study because of prohibitively high computational costs. Nevertheless, as a consistency check, the ensemble described in Figure 11 may be replaced by one with an alternate (random) set of site energies. It is seen that at room temperature the result of near-optimal efficiency changes little under an assumption of different site energies (not shown). This is because the transfer rates at room temperature are influenced more strongly by couplings than by site energies, unless site energy variations are large enough to be comparable to the spectral width of individual chlorophylls (see eq 10). Also, the similarity between the networks of excitation transfer pathways for dipolar and full Coulomb couplings seen in Figure 6 seems to suggest that the general properties of excitation transfer dynamics and therefore also the optimality will not be greatly effected by going from the dipolar to the full Coulomb couplings.

7. Conclusion

The availability of a high-resolution structure of the cyanobacterial photosystem I provides new opportunities to investigate the mechanism of light harvesting in this large pigment−protein complex. In this study, the excitation transfer dynamics at room temperature has been examined starting from an effective Hamiltonian based on interactions between chlorophylls.

As a first approximation, the effect of chlorophyll−protein interactions on the site energies has been ignored. However, we have used the available spectral data to construct a more refined Hamiltonian with limited information on site energies. Also, a prediction on the overall heterogeneity of site energies is made.

The calculated quantum yield and average excitation lifetime at room temperature compare favorably with experimental results. The sojourn expansion method resolves details of excitation migration in PSI, namely, repeated approaches to and escapes from the reaction center. Studying an ensemble of Hamiltonians corresponding to copies of PSI with varying site energies, it is seen that the yield and the lifetime are influenced largely by interchlorophyll couplings and not so much by fluctuations of the site energies at room temperature. The sojourn expansion reveals that the time for a first delivery of excitation to P700 contributes less than half of the average excitation lifetime. At room temperature, about two-thirds of the lifetime results from detrapping events.

However, the low-temperature behavior of PSI is more difficult to describe accurately than the room-temperature behavior. Not only is the low-temperature absorption spectrum impossible to reproduce without a knowledge of chlorophyll site energies, but also overlap integrals contributing to the excitation transfer rates become much more sensitive to the difference between the donor and the acceptor site energies because of the smaller line widths at low temperatures. Furthermore, the broadening of line shapes due to electron−phonon couplings also need to be carefully taken into account at low temperatures because this effect may have a significant impact on the overlap integrals in the framework of Förster theory. Ignoring these contributions results in an unrealistic picture of excitation transfer dynamics at low temperature.

The robustness and optimality of the chlorophyll arrangement in PSI has been examined by means of various computational experiments. On one hand, it is seen that the efficiency of the chlorophyll network of PSI is robust against perturbations such as the pruning of individual chlorophylls or fluctuations of chlorophyll site energies. On the other hand, a study of an ensemble of alternate PSI's with randomly reoriented chlorophyll aggregates shows that the original arrangement actually has a near-optimal quantum yield.

Note Added in Revision

After submission of this paper, we have been informed of a recent calculation of chlorophyll site energies for cyanobacterial PSI.[59] When these site energy values are substituted in the computations outlined above, we obtain at room temperature an average excitation lifetime of 33.9 ps and a quantum yield of 96.6%, which compare favorably with the results given in

TABLE 4: Semiempirical Parameters of the PPP Hamiltonian as Defined in Expressions 33, 34, and 35

	carbon (C)	oxygen (O)	nitrogen (N)
I_k, eV	11.16	17.70	14.12
R_{kk}, eV	11.13	15.23	12.34
γ_0, eV	−2.43	−2.43	−2.43
Z_k	1.0	1.0	1.0
$r_{k,k\pm1}$ (double bonds), Å	1.35	1.35	1.35
$r_{k,k\pm1}$ (single bonds), Å	1.46	1.46	1.46

this paper. The overall width of the distribution of site energies, including the red chlorophylls and P700, is around 260 cm^{-1}, which is larger than the estimate made in this paper of 180 cm^{-1} based on the bulk of the low-temperature spectrum. These new results support our suggestion that the room-temperature excitation transfer dynamics of PSI can be described well without detailed knowledge of site energies. Repeating the optimality study discussed in section 6 also for the set of site energies in ref 59 yields results similar to those shown in Figure 11.

Acknowledgment. The authors thank A. Damjanović, J. Gullingsrud, S. Hayashi, R. Knox, G. Small, E. Tajkhorshid, and R. van Grondelle for useful discussions. This work has been supported by NIH Grants PHS 5 P41 RR05969 and PHS 1 R01 GM60946 and the Fetzer Institute.

Appendix A: Full Coulomb Computation of Interchlorophyll Couplings

Here, we outline the method employed to compute the electronic couplings, $W_{\alpha\beta}$, between two chlorophylls semiempirically. This section follows ref 26 to which the reader is referred for a more detailed treatment.

The electronic coupling between a donor and an acceptor molecule can be written

$$W_{\alpha\beta} = \sum_{i,j\in I_D}\sum_{R,S\in I_A} C^{c}_{ij,RS}\langle\psi^*_\alpha|{}^{00}O^i_j|\psi_\alpha\rangle\langle\psi_\beta|{}^{00}O^R_S|\psi^*_\beta\rangle \quad (32)$$

where I_D and I_A denote the set of atomic orbital indices of the donor and acceptor chlorophylls and $C^{c}_{ij,RS}$ describe the Coulomb integrals involving atomic orbitals labeled by i, j, R, and S. The spin tensors, ${}^{00}O^i_j$ and ${}^{00}O^R_S$, prompt the intramolecular transitions $|\psi_\alpha\rangle \rightarrow |\psi^*_\alpha\rangle$, $|\psi^*_\beta\rangle \rightarrow |\psi_\beta\rangle$. The Coulomb interaction has zero rank, as denoted by the 00 superscript. Therefore, it only proceeds through singlet−singlet transitions. The Coulomb integral, $C^{c}_{ij,RS}$, can be approximated[42] as $S_{ij}(e^2/R_{ij,RS})S_{RS}$, where S_{ij} and S_{RS} are the atomic-orbital overlap integrals and $R_{ij,RS}$ is the distance between the midpoint of atoms i and j and the midpoint of the atoms R and S. As suggested in ref 53, S_{ij} is taken to be 1 when $i = j$, 0.27 when atoms i and j are joined by a chemical bond, and zero otherwise.

To evaluate the transition density matrix elements, one requires the description of the chlorophyll electronic states involved in the excitation transfer process. We choose a semiempirical description for the chlorophyll electronic states as provided by the Pariser−Parr−Pople (PPP) Hamiltonian,[54,55] which has been used earlier in refs 26 and 28. The PPP Hamiltonian

$$H_{PPP} = \sum_{i<j} Z_i Z_j R_{ij} + \sum_{i,\sigma}(-I_i - \sum_{j\neq i} Z_j R_{ij})n_{i\sigma} + \sum_{i\neq j,\sigma} t_{ij}c^+_{i\sigma}c_{j\sigma} + \frac{1}{2}\sum_{i,j,\sigma,\tilde{\sigma}} R_{ij}n_{i\sigma}n_{i\tilde{\sigma}} \quad (33)$$

involves orbitals of π-type only. The creation and annihilation operators, $c^+_{i\sigma}$ and $c_{j\sigma}$, act on mutually orthogonal atomic π-orbitals. The corresponding number operator is given by $n_{i\sigma} = c^+_{i\sigma}c_{i\sigma}$. R_{ij} is the effective electron−electron repulsion integral between an electron in atomic obital at site i and one in orbital at site j, and t_{ij} denotes the resonance integral between atoms i and j. I_i is the effective ionization potential of an orbital at site i. Z_i is the net charge of the core at atom i, which was chosen to be 1. The resonance integral, $t_{\alpha\beta}$, is evaluated according to the empirical formula[56]

$$t_{\alpha\beta} = \gamma_0 + 3.21(r_{ij} - 1.397\text{Å}) \quad (34)$$

where γ_0 is a constant and r_{ij} is the distance between the nuclear sites i and j. The effective electron−electron repulsion integral, R_{ij}, is calculated through the Ohno formula,[57,58]

$$R_{ij} = 14.397\ \text{eV}\left[\left(\frac{2\times 14.397\ \text{eV}}{R_{ii}+R_{jj}}\right)^2 + \frac{r_{ij}^2}{\text{Å}^2}\right]^{-1/2} \quad (35)$$

Assuming the same values of the semiempirical parameters as in ref 26 (listed in Table 4), we perform a SCF-CI calculation, including all single-excited π-orbitals, for the singlet states of a chlorophyll.

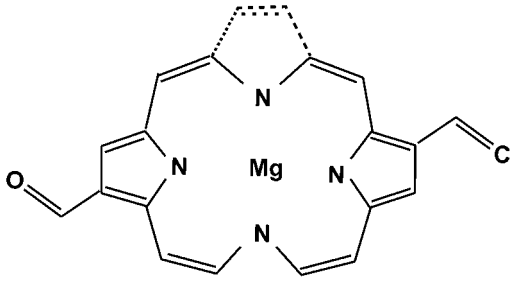

Figure 12. Schematic representation of the conjugated double bonds of the chlorophyll analogue (in solid line) used in the calculations of the couplings. Part of ring II (dotted line) has been removed from the structure (see text).

The chlorophyll electronic structure calculations are based on geometries of a simplified chlorophyll analogue, displayed in Figure 12 (solid line). In this analogue, the double bond of ring II (dotted line in Figure 12) is taken out. Thus, the chlorophyll is almost symmetric about the magnesium atom except that there is a carbon atom at one end and an oxygen atom at the opposite end. For the calculations performed on the analogue structure, the Q_x and Q_y states are easy to identify. However, for the calculations based on the real chlorophyll structure, in which the electronic states are mixed, this identification is difficult. A fully symmetric analogue, with both oxygen atoms at the end, was also proposed in ref 28 on the basis of the same consideration and the error arising from the simplified chlorophyll analogue was shown to be insignificant compared to the systematic errors.

References and Notes

(1) Blankenship, R. E. *Molecular Mechanisms of Photosynthesis*; Blackwell Science: Malden, Massachusetts, 2002.
(2) Gobets, B.; van Grondelle, R. *Biochim. Biophys. Acta* **2001**, *1507*, 80.
(3) Chitnis, P. R. *Annu. Rev. Plant Physiol. Plant Mol. Biol.* **2001**, *52*, 593.
(4) Melkozernov, A. N. *Photosyn. Res.* **2002**, *70*, 129.
(5) Jordan, P.; Fromme, P.; Witt, H. T.; Klukas, O.; Saenger, W.; Krauss, N. *Nature* **2001**, *411*, 909.
(6) McDermott, G.; Prince, S.; Freer, A.; Hawthornthwaite-Lawless, A.; Papiz, M.; Cogdell, R.; Isaacs, N. *Nature* **1995**, *374*, 517.
(7) Miller, K. *Nature* **1982**, *300*, 53.

(8) Koepke, J.; Hu, X.; Münke, C.; Schulten, K.; Michel, H. *Structure* **1996**, *4*, 581.
(9) Sundström, V.; Pullerits, T.; van Grondelle, R. *J. Phys. Chem. B* **1999**, *103*, 2327.
(10) Hu, X.; Ritz, T.; Damjanović, A.; Schulten, K. *J. Phys. Chem. B* **1997**, *101*, 3854.
(11) Hu, X.; Ritz, T.; Damjanović, A.; Autenrieth, F.; Schulten, K. *Q. Rev. Biophys.* **2002**, *35*, 1.
(12) Ritz, T.; Damjanović, A.; Schulten, K. *Chem. Phys. Chem.* **2002**, *3*, 243.
(13) Schulten, K. In *Simplicity and Complexity in Proteins and Nucleic Acids*; Frauenfelder, H., Deisenhofer, J., Wolynes, P. G., Eds.; Dahlem University Press: Berlin, 1999; pp 227−253.
(14) Xiong, J.; Fischer, W. M.; Inoue, K.; Nakahara, M., Bauer, C. E. *Science* **2000**, *289*, 1724.
(15) Blankenship, R. E. *Trends Plant Sci.* **2001**, *6*, 4.
(16) Ritz, T.; Hu, X.; Damjanović, A.; Schulten, K. *J. Lumin.* **1998**, *76*−*77*, 310.
(17) Damjanović, A.; Ritz, T.; Schulten, K. *Int. J. Quantum Chem.* **2000**, *77*, 139.
(18) Prigogine, N. *Self-Organization in Nonequilibrium Systems*; Wiley-Interscience: New York, 1977.
(19) Eigen, M.; Schuster, P. *Naturwissenschaften* **1977**, *64*, 541.
(20) Barkai, N.; Leibler, S. *Nature* **1997**, *387*, 913.
(21) Alon, U.; Surette, M. G.; Barkai, N.; Leibler, S. *Nature* **1999**, *397*, 168.
(22) Humphrey, W.; Dalke, A.; Schulten, K. *J. Mol. Graphics* **1996**, *14*, 33.
(23) Scheer, H. *Chlorophylls*; CRC Press: Boca Raton, Florida, 1991.
(24) Förster, T. *Ann. Phys. (Leipzig)* **1948**, *2*, 55.
(25) Dexter, D. *J. Chem. Phys.* **1953**, *21*, 836.
(26) Damjanović, A.; Ritz, T.; Schulten, K. *Phys. Rev. E* **1999**, *59*, 3293.
(27) Durrant, J. R.; Klug, D. R.; Kwa, S. L. S.; van Grondelle, R.; Porter, G.; Dekker, J. P. *Proc. Natl. Acad. Sci. U.S.A.* **1995**, *92*, 4798.
(28) Damjanović, A.; Ritz, T.; Schulten, K. *Biophys. J.* **2000**, *79*, 1695.
(29) Pålsson, L.-O.; Fleming, C.; Gobets, B.; van Grondelle, R.; Dekker, J. P.; Schlodder, E. *Biophys. J.* **1998**, *74*, 2611.
(30) Zazubovich, V.; Matsuzaki, S.; Johnson, T. W.; Hayes, J. M.; Chitnis, P. R.; Small, G. J. *Chem. Phys.* **2002**, *275*, 47.
(31) May, V.; Kühn, O. *Charge and Energy Transfer Dynamics in Molecular Systems: A Theoretical Introduction*; Wiley: Berlin, 2000.
(32) Louwe, R. J. W.; Vrieze, J.; Aartsma, T. J.; Hoff, A. J. *J. Phys. Chem. B* **1997**, *101*, 11273.
(33) Porter, C. E. *Statistical Theories of Spectra: Fluctuations*; Academic Press: New York, 1965.
(34) Mehta, M. L. *Random Matrixes*, 2nd ed.; Academic Press: San Diego, CA, 1991.
(35) Guhr, T.; Müller-Groeling, A.; Weidenmüller, H. A. *Phys. Rep.* **1998**, *299*, 189.
(36) Sener, M.; Schulten, K. *Phys. Rev. E* **2002**, *65*, 031916.
(37) Damjanović, A.; Kosztin, I.; Kleinekathoefer, U.; Schulten, K. *Phys. Rev. E* **2002**, *65*, 031919.
(38) Barvik, I.; Warns, C.; Neidlinger, T.; Reineker, P. *Chem. Phys.* **1999**, *240*, 173.
(39) Pieper, J.; Rätsep, M.; Jankowiak, R.; Irrgang, K.-D.; Voigt, J.; Renger, G.; Small, G. J. *J. Phys. Chem. A* **1999**, *103*, 2412.
(40) Pieper, J.; Schödel, R.; Irrgang, K.-D.; Voigt, J.; Renger, G. *J. Phys. Chem. B* **2001**, *105*, 7115.
(41) Ritz, T.; Park, S.; Schulten, K. *J. Phys. Chem. B* **2001**, *105*, 8259.
(42) Nagae, H.; Kakitani, T.; Katohi, T.; Mimuro, M. *J. Chem. Phys.* **1993**, *98*, 8012.
(43) Pieper, J.; Irrgang, K.-D.; Rätsep, M.; Voigt, J.; Renger, G.; Small, G. J. *Photochem. Photobiol.* **2000**, *71*, 574.
(44) Brettel, K. *Biochim. Biophys. Acta* **1997**, *1318*, 322.
(45) van Grondelle, R.; Dekker, J. P.; Gillbro, T.; Sundström, V. *Biochim. Biophys. Acta* **1994**, *1187*, 1.
(46) Owens, T. G.; Webb, S. P.; Mets, L.; Alberte, R. S.; Fleming, G. R. *Proc. Natl. Acad. Sci. U.S.A.* **1987**, *84*, 1532.
(47) Gobets, B.; van Stokkum, I.; Rögner, M.; Kruip, J.; Schlodder, E.; Karapetyan, N. V.; Dekker, J. P.; van Grondelle, R. *Biophys. J.* **2001**, *81*, 407.
(48) Holzwarth, A. R.; Schatz, G.; Brock, H.; Bittersmann, E. *Biophys. J.* **1993**, *64*, 1813.
(49) Kennis, J. T. M.; Gobets, B.; van Stokkum, I.; Dekker, J. P.; van Grondelle, R.; Fleming, G. R. *J. Phys. Chem. B* **2001**, *105*, 4485.
(50) Melkozernov, A. N.; Lin, S.; Blankenship, R. E. *Biochemistry* **2000**, *39*, 1489.
(51) Melkozernov, A. N.; Lin, S.; Blankenship, R. E.; Valkunas, L. *Biophys. J.* **2001**, *81*, 1144.
(52) Valkunas, L.; Liuolia, V.; Dekker, J. P.; van Grondelle, R. *Photosynth. Res.* **1995**, *43*, 149.
(53) Weber, W. Ein neues semiempirisces NDDO−Verfahren mit Orthogonalisierungskorrekturen: Entwicklung des Modells, Implementierung, Parametrisierung und Anwendungen. Ph.D. Thesis, Universität Zürich, Philosphische Fakultät II, Zürich, Switzerland, 1996.
(54) Pariser, R.; Parr, R. G. *J. Chem. Phys.* **1953**, *21*, 466.
(55) Pople, J. A. *Trans. Faraday Soc.* **1953**, *42*, 1375.
(56) Schulten, K.; Ohmine, I.; Karplus, M. *J. Chem. Phys.* **1976**, *64*, 4422.
(57) Tavan, P.; Schulten, K. *J. Chem. Phys.* **1986**, *85*, 6602.
(58) Tavan, P.; Schulten, K. *Phys. Rev. B* **1987**, *36*, 4337.
(59) Damjanović, A.; Vaswani, H. M.; Fromme, P.; Fleming, G. R. *J. Phys. Chem. B*, submitted for publication.